PERFORMANCE MODEL OF ELECTRODE TAILORED THIN FILM PIEZOELECTRIC TRANSFORMERS FOR HIGH FREQUENCY SWITCHED MODE POWER SUPPLIES

Sarah S. Bedair, Jeffrey S. Pulskamp, Brian Morgan, Ronald G. Polcawich
U. S. Army Research Laboratory

Abstract: A design and performance model of a 21.4 MHz (190μm x 40μm x 11μm) length extensional thin film piezoelectric resonator using lead zirconium titanate (PZT) is presented as a power transformer. The input and output electrode coverage is used to tailor to various loads for impedance matching and gain. Expected performances specifications including efficiency, power delivery and voltage boosts are reported. The AC/AC performances using electrode tailoring is presented and followed by simulation results of expected AC/DC performances using a voltage doubler configuration (voltage boost of 8.2 at 29% efficiency with a 1MΩ load). This work shows that thin film PTs (<0.01mm^2) performances are comparable to larger (>4mm^2), state of the art thin film magnetic transformer at similar switching frequencies which suffer from high frequency magnetic losses.

Keywords: high frequency power conversion, piezoelectric transformers, electrode tailoring, resonant converters

INTRODUCTION

There is an interest in compact power supply units with a single battery input and multiple voltage outputs for mobile micro-systems [1]. The size of switched mode power supplies are constrained by the large size of the passive components such as inductors and transformers. Implementation of these power conditioning units using COTS switched mode converters would cripple the entire mobile micro-system. Increasing the switching frequency is motivated by reducing the size of the power unit, whereby scaled passive components may be implemented at higher frequencies, further reducing the converter size and weight. Low frequency bulk resonant piezoelectric transformers (< 5MHz) have been implemented in power conditioning units for advantages over magnetic core transformers including high voltage isolation, small size and the absence of induced electromagnetic noise [2]. In this work, the predicted performance of thin film, high frequency piezoelectric resonant transformers (PT) as the passive component in a power converter architecture is evaluated. The current work extends the larger bulk AC/AC and AC/DC performance models to evaluate thin film piezoelectric resonators where electrodes may be lithographically defined for load impedance matching. An array of PT impedance matched to various loads is envisioned providing an ultra-miniature power conditioning unit.

There has been significant research on high frequency piezoelectric resonators for use as high frequency filters and use in low phase noise oscillators. Aluminum nitride resonators have been reported to have a motional resistance, R_m, of 100 Ω with Q = 750 in air at 796 MHz [3]. An aluminum nitride resonator with R_m of 56 Ω, at 224 MHz with Q = 2400 [4] has also been demonstrated. A 1dB compression at 15dBm was reported for a 96 MHz, R_m = 110 Ω, aluminum nitride on silicon resonator [5] showing practical power handling capabilities. Lead zirconium titanate (PZT) on silicon resonators have been reported with R_m = 50Ω, Q = 2023 at 21 MHz [6] with a 32 V/μm bias.

For power converters, power will be delivered to varying loads and load impedance matching is important for efficiency, voltage boost/buck and power delivery. Although there are several challenges with thin film PT including depoling, they present a promising alternate technology to thin film magnetic transformers. The state of the art in thin film magnetic transformers is limited by the magnetic material performances at high frequencies [7]. Table 1 is a comparison of prior work in magnetic micro-transformers using thin film $Ni_{80}Fe_{20}$ [8] [9] and CoNbZr [10]. The transformer measured turns ratio, coupling factor, *k*, gain/efficiencies and size are listed. It is important to note the size of the magnetic transformers, where typical thin film piezoelectric resonators at similar frequencies are at least 2 orders of magnitude smaller in area, therefore, providing a viable technology for future miniature converters.

Ref.	*Turns ratio*	*k*	*Gain/ Efficiency*	*f [MHz]*	*Size mm^2*
[8]	1:1	0.85	NA/31.6%	25	3.8 x1.5
[9]	1:1	0.9	0.63(50 Ω)/NA	10	4 x 1
[10]	8:7.3	0.7	NA/67% (10 Ω)	10	2.4x3.1

Table 1: Survey of prior art and performances of high frequency magnetic transformers.

DESIGN & THEORY

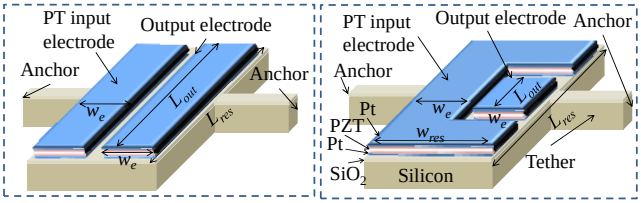

Figure 1: (Left) Illustration of matched input and output electrode coverage in prior art. (Right) Illustration of optimizing the electrode coverage for load impedance matching where the L_{out} x w_e area is traded for a larger input electrode area.

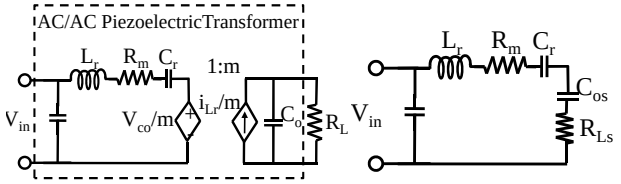

Figure 2: (Left) Small signal series resonant model of the piezoelectric transformer and the load resistance of the subsequent stage. (Right) Illustration of the equivalent parallel to series load.

Piezo-transformer (PT) and Equivalent Circuit

An example thin film piezoelectric resonator is show in Figure 1. Figure 1-left illustrates the design for the 21.4 MHz fundamental length extensional resonant mode previously reported with L_{res} = 190μm, w_{res} = 40μm and w_e = 20 μm [6]. Although the analysis below addresses the electrode tailoring model (illustrated in Figure 1-right) for the fundamental length extensional mode, it can be extended to alternate resonant bulk modes in addition to higher order modes.

Figure 2 shows the small signal equivalent circuit resonant model of the piezoelectric transformer where L_r, R_m and C_r describe PT series resonant equivalent circuit parameters and C_o is the equivalent output capacitance of the transformer [2]. The load resistance, R_L, describes the resistance of the subsequent stage to which power would be transferred. A detailed derivation of the electromechanical properties of lateral bulk mode piezoelectric resonators in [11] yields the following relation for the motional resistance, inductance and capacitance

$$R_m = \frac{n\pi A_x\sqrt{E_i\rho_m}}{2Q}\frac{1}{\eta_{in}\eta_{out}},\quad L_r = \frac{\rho_m A_x L_{res}}{2}\frac{1}{\eta_{in}\eta_{out}}$$

$$C_r = \eta_{in}\eta_{out}\frac{2L_{res}}{n^2\pi^2 E_i A_x} \qquad \text{(1a), (1b), (1c)}$$

where n is the mode number (n = 1 for the analysis below), A_x is the resonator cross-sectional area, E_i the composite modulus, ρ_m the composite density, Q the quality factor, L_{res} the length of the resonator, and η_{in} and η_{out} the input and output electromechanical coupling coefficients, respectively. The electromechanical coefficients are described by

$$\eta_{in} = -E_f d_{31}\int_{Lin}\frac{n\pi}{L_{res}}w_{in}(x)\sin\left(\frac{n\pi x}{L_{res}}\right)dx,$$

$$\eta_{out} = -E_f d_{31}\int_{Lout}\frac{n\pi}{L_{res}}w_{out}(x)\sin\left(\frac{n\pi x}{L_{res}}\right)dx \qquad \text{(2a), (2b)}$$

where E_f is the piezoelectric elastic modulus, d_{31} is the piezoelectric strain coefficient, L_{in} and L_{out} the length of the input and output electrodes, respectively, and $w_{in}(x)$ and $w_{out}(x)$ the widths of the input and output electrodes, respectively. The output capacitance is

$$C_o = \frac{\varepsilon_o\varepsilon_r L_{out}w_{out}}{t_{PZT}} \qquad (3)$$

where ε_o is the permittivity of free space, ε_r the relative permittivity of the thin film PZT, and t_{PZT} the thickness of the piezoelectric film. The mechanical resonance is described by

$$\omega_r = \sqrt{\frac{1}{L_r C_r}} \qquad (4)$$

AC/AC Performance

The equivalent parallel to series conversion of the load C_o and R_L results in,

$$C_{os} = C_o\frac{1+(\omega C_o R_L)^2}{(\omega C_o R_L)^2},\quad R_{Ls} = \frac{R_L}{1+(\omega C_o R_L)^2} \qquad \text{(5a), (5b)}$$

where m in Figure 2 is assumed to be 1 (for isolation). Figure 3 shows the equivalent R_{Ls} versus R_L for varying output electrode coverage, L_{out}/L_{res} x 100%. The following parameters were used: L_{res} = 190 μm, w_{out} = 20 μm, t_{PZT} = 0.5 μm, ε_r = 1000. The peak in efficiency occurs at the peak in R_{Ls}, while the peak in power delivery occurs at $R_m = R_{Ls}$. The normalized power delivered to load is described by

$$\frac{P_L}{|V|^2} = \frac{R_{Ls}}{(R_m+R_{Ls})^2+\left(\omega L_r-\frac{1}{\omega C_r}-\frac{1}{\omega C_{os}}\right)^2} \qquad (6)$$

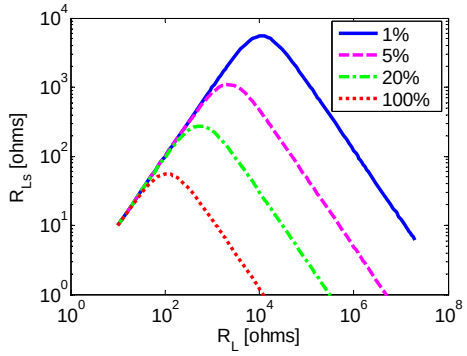

Figure 3: Equivalent series resistance, R_{Ls}, versus R_L with varying electrode coverage, L_{out}/L_{res} x 100%.

where peak power delivered to the load occurs at 50% efficiency and at system resonant frequency of

$$\omega_{\max} = \sqrt{\frac{C_r + C_{os}}{L_r C_r C_{os}}} \tag{7}$$

Depending on the operating regime, i.e. loads either requiring high voltage, low current or low voltage, high current, the performance may be tailored by reducing the output capacitance, C_o, through decreasing the output electrode. Although this comes at a cost of reduced output electromechanical coupling and higher R_m, the tradeoffs in efficiency and boosts over higher R_m are improved under higher resistive load, lower power delivery regimes where voltage boosts are desired. The normalized power delivered to the load, efficiency and voltage gain as a function of R_L are shown in Figure 4 at varying output electrode coverage, 100% x L_{out}/L_{res}. These plots assume the following resonator equivalent circuit conditions of symmetric input and output electrode coverage (L_{out} = L_{res} = L_{in}, $w_{\text{out}}(x)$ = $w_{\text{in}}(x)$): $R_{m\text{-}sym}$ = 50 Ω, $L_{r\text{-}sym}$ = 0.75mH and $C_{r\text{-}sym}$ = 74fF. The figure illustrates the predicted power and gain plots for varying output electrode coverage where the reduced output area is traded with larger input electrode area to maximize η_{in}. The values of R_m, L_r, and C_r are scaled appropriately. For example, in the case of R_m its value is scaled in the following manner

$$R_m = R_{m-sym} \frac{\eta_{in-sym}\eta_{out-sym}}{\eta_{in}\eta_{out}} \tag{8}$$

where $\eta_{in\text{-}sym}$ and $\eta_{out\text{-}sym}$ are evaluated for the case of matched input and output electrodes where w_{in} = w_{out} throughout the matched electrode lengths of L_{in} = L_{out} = L_{res} as illustrated in Figure 1-left.

The normalized power delivered and voltage gain for varying R_L are shown (Figure 4-a, 4-b) for two frequency conditions: mechanical resonance, ω_r, and system resonance, ω_{max}. Therefore, the converter circuit must be tuned according to the system resonance and not the mechanical resonance for maximum power delivery. Figure 4 also illustrates that output electrode coverage may be tailored to maximize voltage gain and power delivery at a trade with efficiency. For example, if 50% efficiency (Figure 4-c) can be tolerated, voltage boosts (normalized power delivered) of 3.53 (156 μW/V^2), 3.47 (750 μW/V^2) and 2.80 (2.6 mW/V^2) may be achieved by designing the output electrode coverage at 100% x L_{out}/L_{res}=1%, 5% and 20% for loads of 80 kΩ, 16 kΩ and 3 kΩ, respectively. If a 1:1 isolation is desired, Figure 5 shows the predicted efficiencies at the corresponding R_L and optimized electrode coverage. Peak efficiencies of 77%, 62%, and 49% is expected for $R_{m\text{-}sym}$ = 50Ω, 100Ω, and 150Ω, respectively. These are predicted for R_L = 10kΩ, 14kΩ and 20kΩ, respectively.

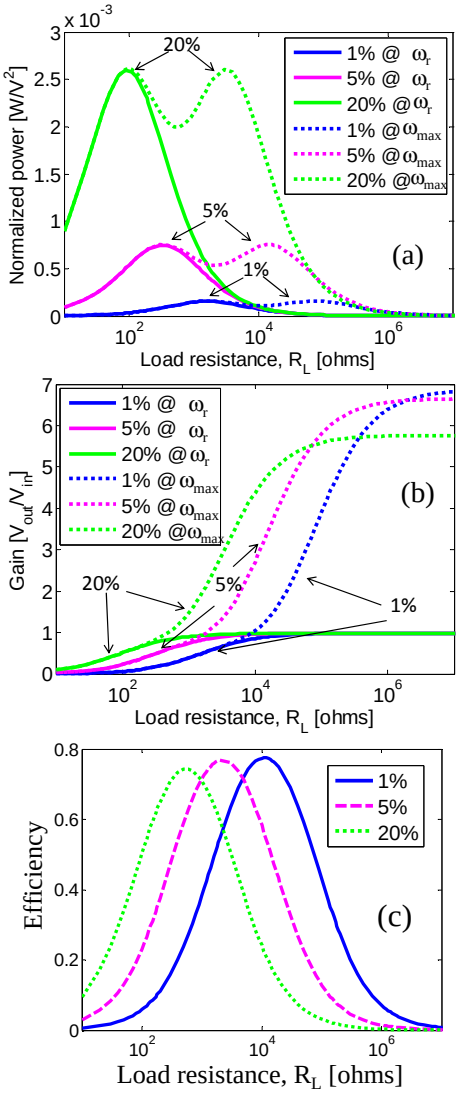

Figure 4: (a) Normalized power delivered to the load, (b) voltage gain and (c) efficiency versus R_L.

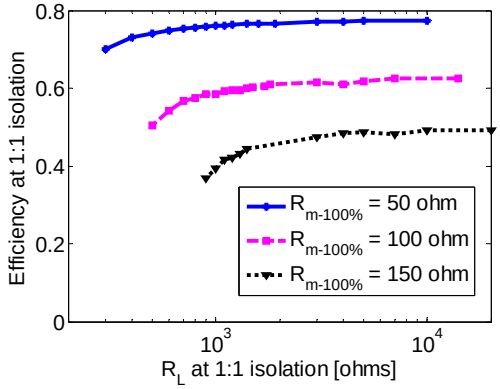

Figure 5: Expected efficiency versus R_L for 1:1 isolation where each point represents the optimized electrode design.

AC/DC Performance

Simulations (using PSpice) of the PT in an AC/DC voltage doubler configuration (Figure 6) were performed. The PT parameters were extracted from $R_{m\text{-}sym}$ = 50 Ω, $L_{r\text{-}sym}$ = 0.75mH and $C_{r\text{-}sym}$ = 74fF. If a low current draw, bias voltage is needed, then the V_{in} voltage can be capacitively coupled to the PT actuating voltage. A filter capacitor is implemented in the design for reducing the ripple. For the simulations, the ripple requirement is held constant at 0.4% and C_{filter} on the output is scaled appropriately for each value of R_L. For each simulation, the optimal drive frequency was used according to Eq. 7 where the effective C_o and, subsequently, C_{os} does depend on C_{filter} and the diode threshold voltage. A detailed derivation for this may be found in [12]. Expected AC/DC performances listed in Table 2 show voltage gains up to 8.2 at 29% efficiency and 0.4% ripple.

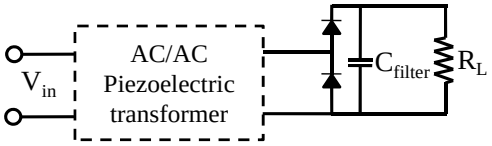

Figure 6: AC/DC PT used in a voltage doubler configuration.

L_{out}/L_{res} *100%	R_L [kΩ]	C_{filter} [nF]	AC/DC gain	% ripple	Efficiency
5%	16	0.625	2.12	0.4	61%
1%	80	0.125	2.17	0.4	61%
1%	100	0.01	8.2	0.4	29%

Table 2: Simulated (PSpice) performances.

CONCLUSIONS

In this paper, the performance of thin film, high frequency piezoelectric transformers as a passive component with a 190μm x 40μm x 11μm volume in a power converter is evaluated. The AC/AC and AC/DC performances were evaluated with varying R_L, whereby electrode tailoring would provide proper impedance matching. If $R_{m\text{-}sym}$ = 50 Ω at 21 MHz can be achieved, a 1:1 isolation at 77% efficiency is predicted with a resonant passive component. An AC/DC voltage boost of 8.2 at 29% efficiency with a 1MΩ load is expected. It is clear that transformer performance can be enhanced by reducing R_m. Significant reductions in motional resistance, beyond the lowest reported values (~50 Ω), appear feasible. Such reductions are expected through continued improvements in quality factor, piezoelectric coefficients, and geometry optimization. This technology would provide a viable alternative to high frequency, micro-machined magnetic transformers which are, at the least, 2 orders of magnetic larger than thin-film, piezoelectric resonant transformers.

REFERENCES

[1] Morgan B, Bedair S, Nothwang W, Arnold D, Meyer C, Bowers B, Sopeju A, Dougherty C, Lin X, Bashirulla R 2009 Micro-power requirements & conversion for autonomous microsystems *NATO Specialist Meeting on Energy Technologies and Energy Management for Portable Power Systems for Military Applications*, Slovenia, May 4-5, 2009

[2] Ivensky G, Zafrany I, Ben-Yaakov S 2002 Generic operational characteristics *IEEE Trans. On Power Electronics*, **17** 1049-1057

[3] Olsson RH III, Flemming JG, Wojciechowski KE, Baker MS, Tuck MR 2007 Post-CMOS compatible aluminum nitride MEMS filters and resonant sensors *IEEE Freq. Cont. Symp, 2007* 412-419

[4] Piazza G, Stephanou PJ, Pisano AP 2006 Piezoelectric aluminum nitride vibrating contour-mode MEMS resonators *JMEMS*, **15**, 1406-18

[5] Abdolvand R, Mirilavasani H, Ayazi F 2007 A low-voltage temperature-stable micromechanical piezoelectric oscillator *14th Intl C onference on Solid State Sensors Actuators and Microsystems, Transducers 2007* 53-56

[6] Chandrahalim H, Bhave S, Polcawich R, Pulskamp J, Judy D, Kaul R, Dubey M 2008 *Applied Physics Letters*, **93**, 233504-1

[7] Yun E, Jung M, Cheon C, Nam HG 2004 Microfabrication and characteristics of low-power high-performance magnetic thin-film transformers *IEEE Trans. Magnetics*, **40** 65-70

[8] Park J, Bu J 2003 Packaging compatible microtransformers on a silicon substrate *IEEE Trans. On Advanced Packing*, **26** 160-164

[9] Xu M, Liakopoulos T, Ahn C, Han S, Kim H 1998 A microfabricated transformer for high-frequency power or signal conversion *IEEE Trans. On Magnetics*, **34** 1369-1371

[10] Yamaguchi K, Sugawara E, Nakajima O, Matsuki H, Murakami K 1993 Load characteristics of a spiral coil type thin film microtransformer *IEEE Trans. Magnetics* **29** 3207-3209

[11] Ho G, Abdolvand R, Sivapurapu A, Humad S, Ayazi F 2008 Piezoelectric-on-silicon lateral bulk acoustic wave micromechanical resonators *J. Microelectromechanical Systems* **17** 512-520

[12] Ivensky G, Shvartsas M, Ben-Yaakov S 2004 Analysis and modeling of a voltage doubler rectifier fed by a piezoelectric transformer, *IEEE Trans. On Power Electronics* **19** 542-549